Coastal Engineering 211 (2026) 105075

Contents lists available at ScienceDirect

Coastal Engineering

journal homepage: www.elsevier.com/locate/coastaleng

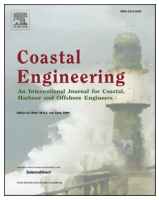

Storm-induced sediment transport at a small tidal inlet

Tansir Zaman Asik [a,*], Duncan FitzGerald [a], Danghan Xie [b], Ioannis Y. Georgiou [c], Zoe Hughes [a], Silke Tas [d]

[a] Department of Earth and Environment, Boston University, Boston, MA, USA
[b] Department of Geographical Sciences, University of Maryland, College Park, MD, USA
[c] The Water Institute, New Orleans, LA, USA
[d] Hydrology & Environmental Hydraulics Group, Wageningen University and Research, Wageningen, Netherlands

ARTICLE INFO

Keywords:
Tidal inlet
Sediment transport
Storms
Numerical models
Hurricane Bob

ABSTRACT

Evaluating sediment transport through tidal inlets is critical for understanding shoreline and backbarrier evolution and for maintaining tidal exchange and vessel navigation. Storm-driven sedimentation is important in determining long-term backbarrier sediment budgets and ecosystem evolution, particularly with the forecasted increase in frequency and magnitude of storms under a regime of climate change. The primary objective of this study is to investigate sediment dynamics during storm and normal tidal conditions and predict net sediment deposition patterns at Allens Pond Inlet, a small inlet in southern Massachusetts. Small inlets (width <100 m) represent an understudied tidal system even though small inlets commonly out-number large inlets along coasts. A hydro- and morpho-dynamic model, Delft3D, was employed to simulate tides, storm-generated currents, and sediment transport. An Acoustic Doppler Current Profiler and water level logger were deployed for model input and validation. Sediment samples from the study area reveal a gradient of fining grain size from the inlet entrance to the backbarrier channels, indicating landward sediment transport. Hydraulic measurements demonstrate a correlation between tidal range and current velocities and confirm that spring tidal ranges produce dominant flood-dominance of the system. Moreover, our modeling results show that storm events significantly enhance sediment influx due to higher order current velocities at the inlet and in backbarrier tidal channels. Our findings explain the formation and landward migration of flood-oriented bedforms, point bars, and tidal deltas suggesting that backbarrier of small inlets are sediment sinks.

1. Introduction

Tidal inlets are dynamic systems that provide a critical connection between the coastal ocean and backbarrier environments, including lagoons, bays, salt marshes and estuaries. Tidal inlets are a primary component of barrier island chains, which are found along every continent except Antarctica (FitzGerald and van Heteren, 1999) and comprise ~10% of world's open-ocean shoreline (Stutz and Pilkey, 2001). Tidal inlets play an essential role in regulating nutrient exchange, discharge of organic detritus, distribution of sediment, and shoreline dynamics (FitzGerald, 1996; Senthilkumar et al., 2017). Inlets are particularly significant in supporting coastal ecosystems, influencing sand reservoirs, and dictating backbarrier hydrodynamics (Hayes and FitzGerald, 2013).

Depending on the size and type of backbarrier basin and its hypsometry, inlets can be flood or ebb dominant based on distortions of the tidal wave. Tidal asymmetries leading to longer ebb versus flood durations produce net sediment transport trends (Boon III and Byrne, 1981; Dronkers, 1986a,b; Friedrichs and Aubrey, 1988). Ebb-dominant inlets, exhibiting shorter ebb durations, tend to remove the sand that enters the inlet by waves and flood-tidal currents, whereas flood-dominant inlets tend to import sediment and enlarge sand shoals in the backbarrier (Boothroyd et al., 1985).

The importance in understanding sediment transport along sandy shorelines during this period of climate change and global warming has grown in recent years due to the predicted increase in storm frequency and magnitude (Knutson et al., 2015; Kossin et al., 2020). This is particularly true for tidal inlets because of their effects on regional sediment budgets and long-term coastal resilience (FitzGerald et al., 2006; Dissanayake et al., 2012). Moreover, Pang et al. (2023) have discussed how climate change accelerates coastal erosion and increases the frequency and intensity of coastal flooding. Recently, research has

* Corresponding author.
E-mail address: tansir@bu.edu (T.Z. Asik).

https://doi.org/10.1016/j.coastaleng.2026.105075
Received 4 March 2026; Received in revised form 21 May 2026; Accepted 22 May 2026
Available online 5 June 2026

focused on storm-generated sediment transport at tidal inlets using hydrodynamic modeling based on conceptualized inlet and basin systems and hypothetical meteorological and physical conditions (e.g., Georgiou et al., 2024). Additional research has been conducted at specific tidal inlets using field data (e.g., Baranes et al., 2023) and hypothetical storm conditions (Castagno et al., 2018). These investigations have shown that storms can overprint the normal flushing regime of ebb dominant inlet channels and, during short timeframes (hours), transport sediment into the backbarrier (Castagno et al., 2018; FitzGerald et al., 2022). Still, the mechanisms and volumes of sand involved during storm events are poorly understood.

Most storm-related investigations of sediment transport at these systems have treated moderate to large-sized inlets (width + 300 to > 1 000 m), whereas small inlets (established here as having width <100 m) have been largely neglected (Duong et al., 2017; Chan, 2023). This study looks at the storm hydrodynamics and sediment transport processes at Allens Pond Inlet along the microtidal coast of Buzzards Bay, Massachusetts (Fig. 1). This is an ideal site for studying coastal processes at small tidal inlets including the interactions among tidal and wave-generated currents, sediment transport, and effects of storms. Small tidal inlets, like Allens Pond Inlet, often contain weaker tidal currents than mesotidal systems because of smaller tidal prisms and less tidal exchange (Duong et al., 2017). Mesotidal inlets usually have moderately deep channels (>8 m; Barwis, 1976) and tend to stabilize in semi-consolidated sediment. Along rocky or glaciated coasts, inlets are commonly situated next to bedrock outcrops or resistive till sediment (FitzGerald, 1993). Conversely, small tidal inlets have shallow channels and are vulnerable to changes in hydrodynamic and sediment transport, especially during storms when increased longshore transport can lead to rapid inlet migration and potential closure (FitzGerald, 1996; Mallinson et al., 2008; Hayes and FitzGerald, 2013; Duong et al., 2017).

To illustrate the importance of small tidal inlets (width <100 m) versus large inlets (width >100 m) along barrier coasts, we have examined their relative distribution along structurally controlled shorelines, including the coasts of Maine and Connecticut in New England, and in coastal plain settings (South Carolina, Georgia, west coast of Florida, Algarve Portugal) (Table 1). This examination is not meant to be an exhaustive analysis, rather we show that small inlets comprise a significant percentage of the total number of inlets along barrier coasts ranging from 73% in Maine and 72% in Connecticut to 34% in South Carolina, 15% in Georgia, 29% along the west coast of Florida, and 67% in Algarve, Portugal in coastal plains settings. It is acknowledged that along some barrier island chains, including the West and East Frisian Islands in the North Sea and Georgia Bight barriers along the Atlantic coast, are composed chiefly of large tidal inlets with very few small inlet systems. However, the abundance of small inlets along the world's barrier coast indicates their importance and relevance in understanding their dynamics, especially during storms.

Our study aims to quantify the volume of storm-driven sediment transport at Allens Pond Inlet. We do this by simulating storm events and evaluating tidal current vectors and sediment transport pathways. This has been supplemented with hydrodynamic, morphologic and sedimentologic field observations. A key research question focuses on how storm surges coupled with flood-directed currents drive sediment inland

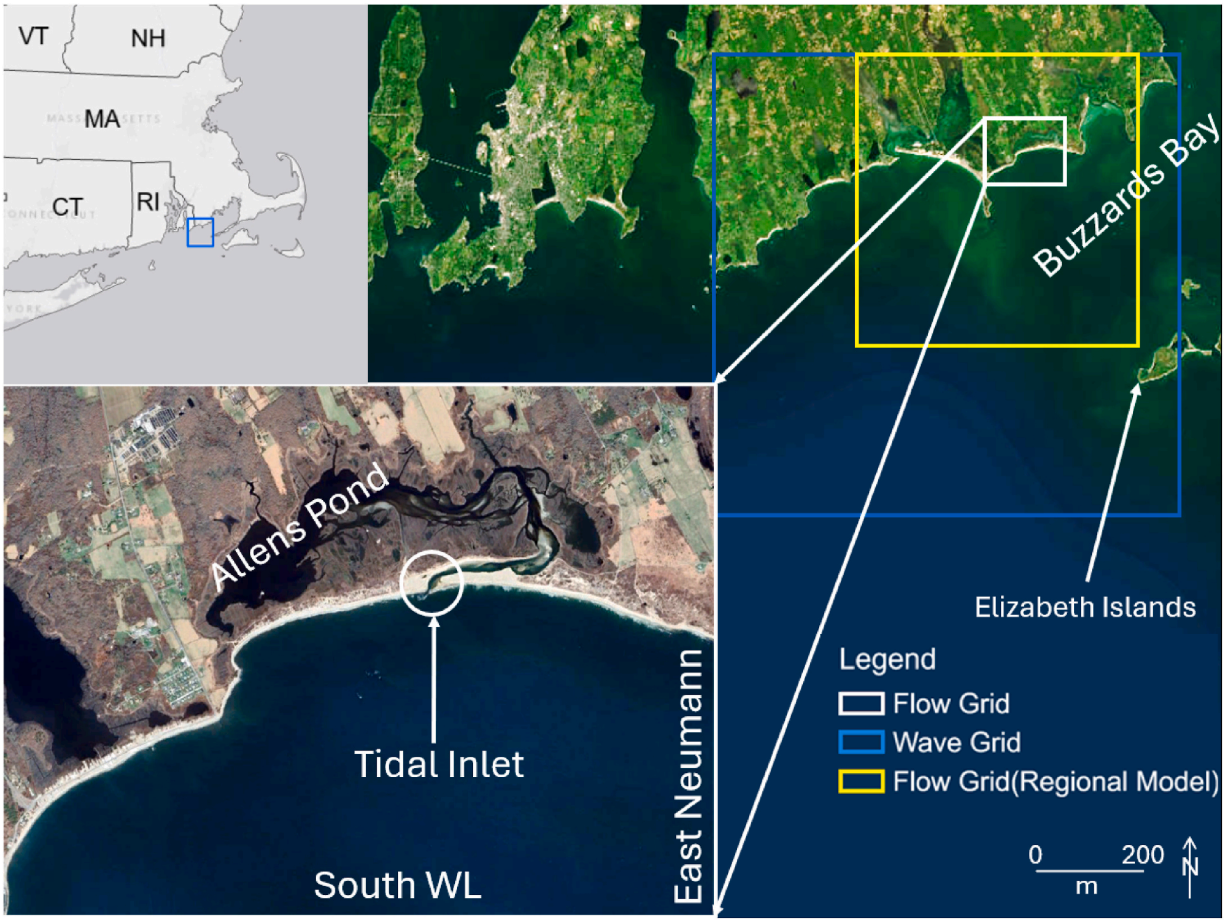

Fig. 1. Buzzards Bay and Allens Pond along the New England coast in Massachusetts, USA. The blue and yellow rectangles show the regional wave and flow domains, respectively used in the Delft3D model (Xie et al., 2024a). The white rectangle is the finer-scale nested domain where the Allens pond and its inlet (white circle) is located. The nested model boundaries (South WL and East Neumann) are also shown in the white rectangle. (For interpretation of the references to colour in this figure legend, the reader is referred to the Web version of this article.)

Table 1
Regional distribution of small and large tidal inlet characteristics along selected coasts.

Region	Coast Name	Coastline Length (km)	Total Tidal Inlets	Large Tidal Inlets (width >100 m)	Small Tidal Inlets (width <100 m)	Percentage of Small Tidal Inlets
Northeast USA	Maine	120	26	7	19	73%
	Connecticut	150	14	4	10	72%
Southeast USA	Georgia	150	7	6	1	15%
	South Carolina	300	12	8	4	34%
	West Coast of Florida	300	70	50	20	29%
Southwest Europe	Southwest Coast of Portugal	100	9	3	6	67%

(Georgiou et al., 2024) and deposit it on flood deltas as has been documented at Essex Inlet in Massachusetts (FitzGerald et al., 2022). Moreover, a modeling study by Castagno et al. (2018) showed that during storms the movement of sediment at inlets along the Virginia coast was differentiated according to grain size with medium to coarse silt being imported, and fine sand being exported from the system. The differences in the findings of these studies emphasizes the need for further study of storm processes at tidal inlets using both field data and numeric modeling. In this study, we model the historical storm of Hurricane Bob (1991) and a significant extratropical storm in November 2022 that impacted the northern Buzzards Bay coast, compared to normal tide condition. The model is validated using nearby hydrodynamic observations. We look at the hydrodynamic storm signature as well as net sand transport trends, which are corroborated by sedimentologic and morphologic field data. This research contributes to the growing literature on microtidal systems (Zhu and Wiberg, 2022) and small tidal inlets (e.g., Duong et al., 2017; Chan, 2023) and offers practical insights for coastal managers striving to preserve these dynamic and ecologically valuable environments amid changing climates (Duong, 2021; Chan, 2023).

2. Setting and methods

In this section, we provide a description of the physical setting of the study area and methodologies employed to study sediment dynamics at Allens Pond Inlet. We utilize the Delft3D modeling platform (Lesser et al., 2004) to simulate hydrodynamics and sediment transport under various conditions, validated by field data including sediment samples, water elevations, and Acoustic Doppler Current Profiler (ADCP) measurements. Model setup, validation procedures, and modeling scenarios are described below.

2.1. Study area

The east-west structural grain of Western Buzzards Bay, Massachusetts (USA), is manifested by a series of north-southward trending ridges and valleys, producing a coastal morphology dominated by promontories and elongated embayment. Where there was sufficient offshore glacial-fluvial sediment, the Holocene transgression move sand onshore creating barriers, tidal inlets, estuaries, and extensive marsh systems (Fig. 1). Allens Pond Inlet, which connects the coastal ocean to Allens Pond and its salt marsh, has formed between two bedrock anchored spit systems. The inlet is approximately 3-m deep at highwater and 50 to 90 m wide depending upon its position along the barrier. Historical aerial photographs and maps of the region dating back to 1934 demonstrate that the inlet is highly dynamic and migrates from the east to the west against the dominant west to east longshore transport direction (FitzGerald et al., 1987; also see Fig. S1a and S1b). The inlet migrates updrift (west) because the ebb-tidal currents preferentially erode the western inlet shoreline. Eventually, as the eastern spit elongates and the inlet migrates west, the efficiency of the hydrodynamic connection between the coastal ocean and backbarrier system diminishes. This leads to a reduction in the tidal prism and closure of the inlet at a far westerly position. In the past, the cycle of migration, inlet closure or near closure, and reopening to the east during a high energy storm occurred naturally once every 5 to 7 years (FitzGerald et al., 1987; see Fig. S1a and S1b). However, during the past ~25 years, when the inlet reaches a far westerly position, a new channel is artificially cut about 500 to 600 m to the east through the eastern spit every 4 to 5 years. A well-developed open connection to the coastal ocean is vital for the health of Allens Pond backbarrier ecosystem.

Tides in the study area are semi-diurnal with a range 0.5 m during neap tides increasing to 1.3 m during spring tide conditions (NOAA, 2025). The average deepwater wave height is approximately 1.0 m with a peak wave period of 7.1 s (NDBC, 2025). Due to the protection by the Elizabeth Islands (location in Fig. 1), the northern Buzzards Bay shoreline only receives large waves approaching from the south to the southwest. The micro-tidal nature and low wave energy of western Buzzards Bay leads to the study area being dominated by infrequent, moderate to large-magnitude storms that significantly impact the overall sediment transport patterns (FitzGerald et al., 1992; Xie et al., 2024a, b). Between 1851 and 2013, the National Oceanic and Atmospheric Administration (NOAA) hurricane database records 55 hurricanes impacting southern New England. Among these, Hurricane Bob in 1991 stands out as relatively recent and significant storm generating a storm surge of about 2.8 m and peak deepwater storm waves exceeding 8 m (Sun et al., 2013). Such extreme storm events have caused considerable sediment transport and shoreline changes in the region (Cheung et al., 2007). During Hurricane Bob (1991) as well as the 1938 Hurricane (see description in Avilés, 2014), overwashing of the barrier and formation of extensive washover fans occurred up and down the coast (Cheung et al., 2007), including the entire marsh as shown in Fig. S2. This washover phenomena is common in the barrier island systems along the New England coastline (FitzGerald et al., 1987; Donnelly et al., 2001). In addition to hurricanes, this region undergoes erosion, flooding, and structural damage during extratropical cyclones with winds and waves from the southwest (Zhang et al., 2020; Xie et al., 2024a, 2024b).

2.2. Field data collection

To determine the hydrodynamic character of Allens Pond inlet, we deployed a suite of instruments, including an Acoustic Doppler Current Profiler (ADCP) within the inlet channel (location in Fig. 2A) that measured depth-resolved velocities and a high-resolution water-level logger inside the pond (Fig. 2A) that recorded tidal elevation. An RBR sensor was sited 3 km offshore of the inlet (Fig. 2A) that provided continuous measurements of water levels and wave conditions, that served as boundary forcing for the numerical model. Together, these synchronized datasets provided a comprehensive view of hydrodynamics that included a detailed record of the extratropical storm in November 2022. We also validated the model during that storm and discussed it in section 2.4.

To characterize sedimentological patterns across the inlet system, we collected 31 surface sediment samples from the spit through the inlet channel and onto adjacent shoals and bars up to the pond (Fig. 2B). Mean grain size and sorting were determined using Folk and Ward (1957) formulas. Finally, the extent of hurricane overwash deposition was defined by 17 cores augered the backside of the barrier system

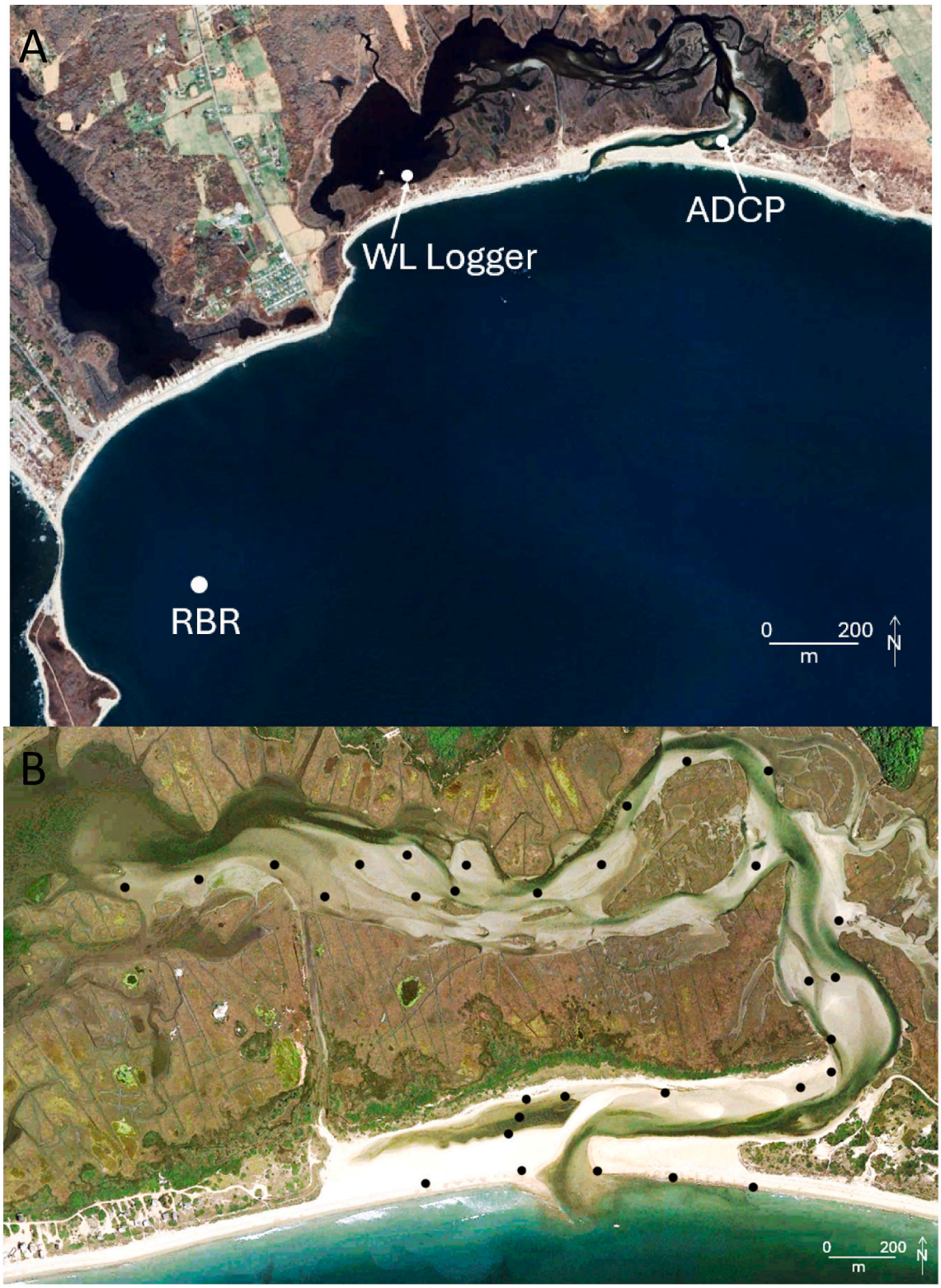

Fig. 2. (A) Locations of deployed instruments, including the ADCP in the inlet channel, the water level (WL) logger inside the pond, and the offshore RBR. (B) Locations of the 31 sediment sample collections, shown as black dots across the spit, inlet channel, and adjacent shoals and bars.

(Fig. S2 in SI).

2.3. Model setup

To study coastal hydrodynamics and sediment transport during non-storm and storm conditions, we used a two dimensional open-source hydrodynamic and sediment transport model, Delft3D, that simulates unsteady flow and transport phenomena under tidal and wave forcing (Lesser et al., 2004). Delft3D-FLOW solves the depth-average shallow water equations to simulate water levels and current velocity (Lesser et al., 2004) and Delft3D-WAVE simulates wave propagation, dissipation, and wave-current interactions based on the third-generation

spectral wave model 'Simulating WAves Nearshore (SWAN)' (Booij et al., 1999). We employed an online-coupled Delft3D-WAVE and Delft3D-FLOW setup with overlapping grids (Fig. 1). This approach allows the model to account for the effects of flow on waves through wave set-up, current refraction, and enhanced bottom friction, as well as the effects of waves on currents through wave forcing and enhanced bed shear stress (Deltares, 2014). Sediment transport within the model was simulated using the van Rijn et al. (2004) formulation, based on the TRANSPOR2004 (van Rijn et al., 2004), with bed-load transport representing the dominant mode of sediment transport in this system. All model parameters related to Delft3D-FLOW, Delft3D-WAVE, and sediment transport are provided in Table S1 of the Supporting Information.

To obtain an efficient simulation, we implemented a nested modeling approach in which a high-resolution refined model is embedded within a coarser regional model. The regional model was validated by Xie et al. (2024a) and includes a flow domain (yellow box in Fig. 1) and a wave domain (blue box in Fig. 1) with a nearshore grid resolution of 40 × 40 m and 80 × 80 m (X × Y directions), respectively. The regional model provides boundary conditions for the refined model, which has a finer flow grid resolution of 5 × 5 m (white box in Fig. 1). And the wave domain contains the same grid resolution as the regional model domain but the finer grid resolution (10 × 10 m) over the nested flow domain (white box in Fig. 1). Overall, the refined flow model domain comprises 858 × 620 grid cells with one offshore water-level boundary on the southern side and a Neumann boundary on the eastern side (Fig. 1). The wave model grid consists of 468 × 388 cells with a single southern boundary providing incident wave forcing. Wave boundary inputs for Allens Pond model include wave height, wave period, and wave direction, as well as wind speed and wind direction, taken from the regional model forcing data.

The bathymetry for the regional model is based on the Continuously Updated Digital Elevation Model (CIRES, 2014; Amante et al., 2023). For the finer nested Allens Pond domain, the latest LiDAR data from 2018 was used as bathymetry in the nested model (OCM Partners, 2018). Because our collected hydrodynamic data was in 2022, the inlet location in 2018 (Fig. S1b in SI) was corrected manually to the inlet location in 2022 (Fig. S1b in SI) in the bathymetry, and the corrected bathymetry data was used in the nested model (Fig. 3). We updated the 2018 LiDAR bathymetry to match the 2022 inlet configuration by delineating the 2018 inlet polygon and copying its elevation field to the 2022 inlet position. The 2018 inlet channel was then infilled by interpolating elevations from the adjacent spit and surrounding bed. Finally, we applied the Delft3D bathymetry smoothing tool to remove artificial steps introduced by the polygon transfer. The updated bathymetry was visually checked and corrected to achieve physically realistic elevation gradients across the updated inlet and spit.

A spatially uniform Chézy bed roughness of 50 $m^{1/2}/s$ is used in the model, following our previous modelling studies in this region (Xie et al., 2024a, 2024b). For the regional and nested Allens Pond models, 200 sediment samples covering areas from deepwater (~15 m water depth) to the beach and backbarrier system were collected and sieved to determine the median grain size (d_{50}) to input into the model. The average d_{50} across the samples was approximately 230 μm (Xie et al., 2024b). Because the main objective of this study was to identify the processes and volumes of medium to fine sand that are imported from the coastal ocean or exported from the backbarrier system through the tidal inlet, we used a median grain size (d_{50}) value 230 μm (medium to fine sand size).

For the nested Allens Pond model, a single sediment layer with a thickness of 5 m was used to avoid limiting erosion (Hanegan et al., 2023). For tracking the influx and outflux of sediment through the inlet, the same thickness and grain size were identified differently, (i.e., inside and outside of the inlet). Additionally, we collected 31 sediment samples from the inlet and main channel, flood deltas and other shoals within backbarrier of Allens Pond (Fig. 2B). Samples were sieved, and mean grain size and sorting (Φ) were calculated using Folk and Ward (1957) grain size statistics (Fig. 2B and S3). Grain size and sorting distributions helped to identify sediment transport trends.

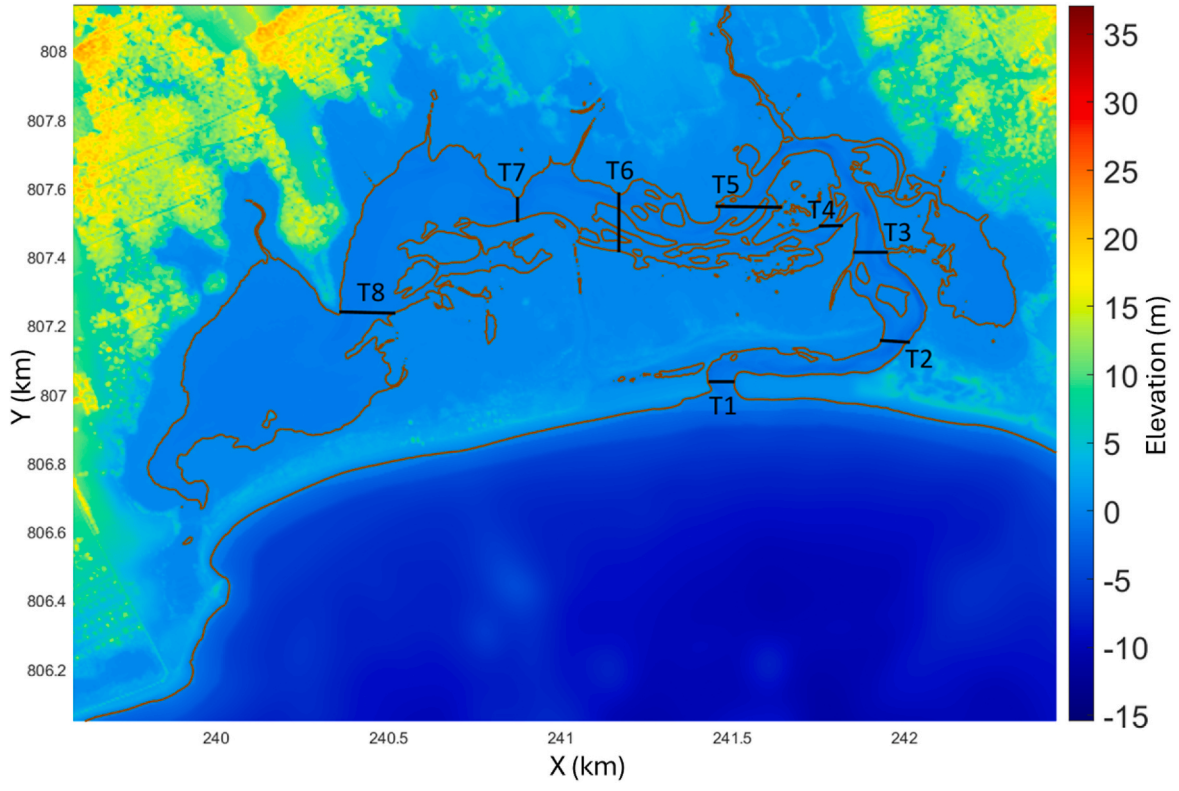

Fig. 3. Bathymetry for the inlet system was extracted from high-resolution LiDAR data. Sediment fluxes were calculated at eight cross-sectional transects (T1–T8) to quantify spatial variations in sediment transport through the inlet and adjacent shoals.

2.4. Model validation

The regional model is validated by comparing data output with two ADCP time series and 43 validation points extracted from the NACCS Coastal Hazards System (Xie et al., 2024a). To validate the nested Allens Pond model, water elevations were compared with high-frequency water level data obtained from the ADCP and Water Level Logger (Fig. 2A) that were installed in the inlet channel and inside the pond, respectively (locations shown in Fig. 2A). The nested model was validated using the water level data as the model boundary obtained from the RBR (location in Fig. 2A). The comparisons of water level and velocity between model output and field observations are shown in Fig. 4. We calculated the model skill index using the validation approach proposed by Willmott (1981), to evaluate the nested model performance. The skill index is defined as:

$$\text{Skill} = 1 - \frac{\sum |X_D - X_S|^2}{\sum \left(|X_D - \overline{X_S}| + |X_S - \overline{X_S}|\right)^2} \quad (1)$$

Where, X_D is the nested Delft3D model output and X_S is the measured data from ADCP and Water Level Logger, both of which are applied herein at hourly intervals. $\overline{X_S}$ is the temporal average of the data points from measurements. The skill index ranges between 0 and 1, where 1 indicates a perfect match between the model output and reference samples, and 0 indicates a complete failure to capture the expected behavior. Previous research suggests that a skill index higher than 0.7 to 0.8 represents a reasonable prediction (Willmott, 1981). Results indicate that our nested model could effectively capture changes in water level both at the inlet channel and inside the pond location; the skill index value (=0.98) for both the locations indicates the model acceptability (Fig. 4A and B). We also calculated the coefficient of determination, R^2 value for both locations, and the values are also in good range at the channel (R^2 = 0.93) and in acceptable range inside the channel (R^2 = 0.94) (Fig. 4A and B) (Moriasi et al., 2007). In addition to water levels, our nested model captures the velocity recorded by ADCP at the inlet channel (Fig. 4C). The skill index and the coefficient of determination, R^2 value for the velocity comparison are 0.84 and 0.66, respectively, which fall within the range commonly considered satisfactory for coastal hydrodynamic model evaluation (Fig. 4C) (Moriasi et al., 2007).

For validating the nested model using the large regional model, we have taken a common grid point both in the nested and the regional domain and compared the water level and velocity during November 2022 storm and Hurricane Bob. The point location and the other parametric comparisons are shown in Fig. S4 in the SI. These comparisons demonstrate that the nested model is performing well in simulating water levels as recorded by the field instruments (Fig. S4b–S4e).

2.5. Model scenarios

We ran three scenarios for the nested Allens Pond Model: (i) normal tide conditions (ii) moderate extratropical storm in November 2022, and (iii) extreme storm Hurricane Bob in 1991. The extreme scenarios were previously processed and validated in the regional model, of Xie et al.

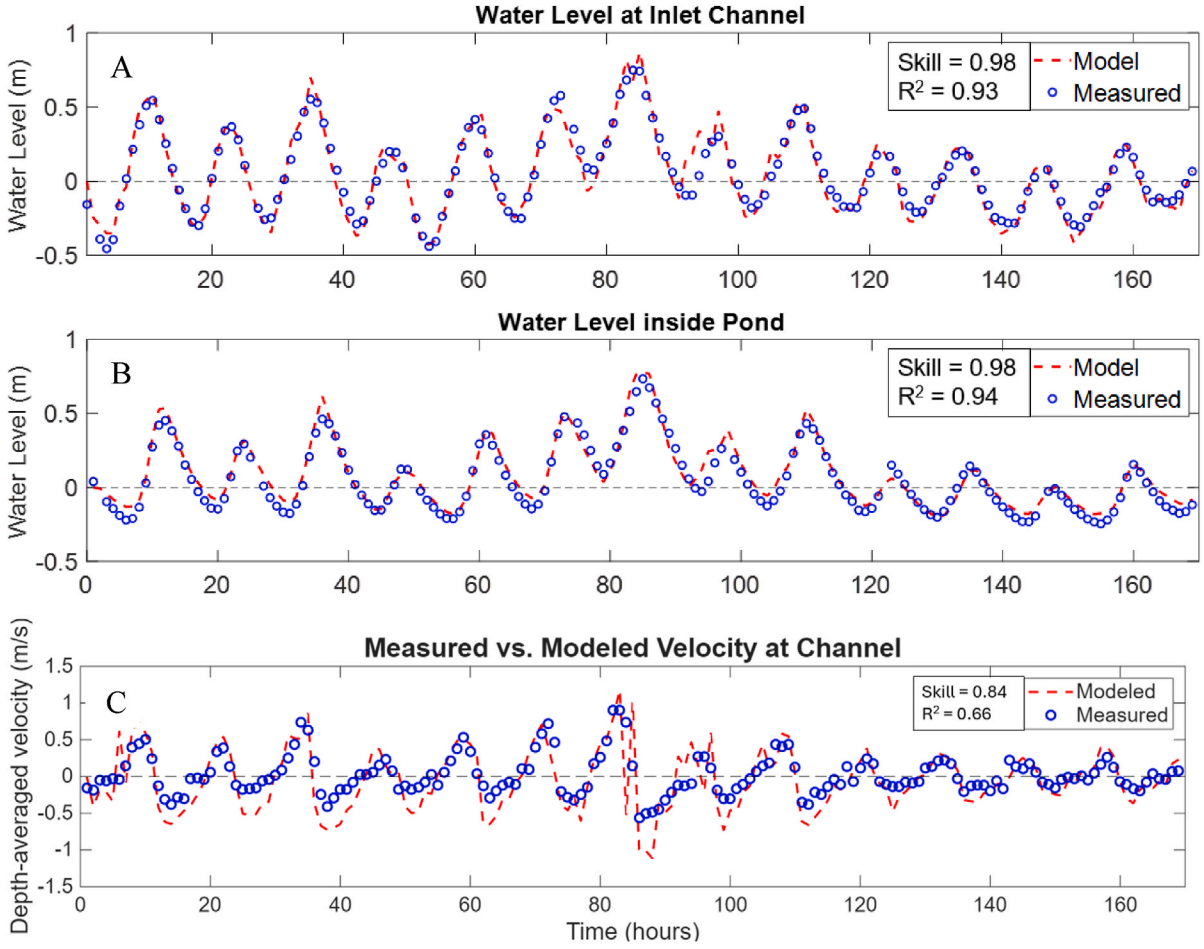

Fig. 4. Temporal comparisons between model-generated and measured water-level for (A) inlet channel and (B) inside the pond, as well as (C) velocity for the inlet channel, including their corresponding skill indexes and R^2 values. Positive velocity indicates flooding currents, while negative velocity indicates ebb currents. The locations of the ADCP and water-level logger are shown in Fig. 2A.

(2024a, 2024b). The resulting water levels from the regional model are used to provide boundary conditions for the nested model. Specifically, the water level along the southern boundary of the nested domain is extracted directly from the corresponding regional model simulations (Fig. 1). The locations of the water level extractions and the time-series of water levels for the three scenarios are shown in Fig. S9 in SI.

3. Results

Our results are provided in four sections: 1. gage measurements of tidal current dominance, 2. modeled hydrodynamics and morphological effects of surge overtopping the barrier, 3. modeled sediment transport in tidal channels, and 4. corroborating field observations. Modeled hydrodynamics show perturbations of tidal wave propagation through the system under normal tides, moderate storms, and extreme storm events. Likewise, modeled sediment transport for the different conditions provide sediment fluxes across eight transects. Finally, grain size trends, bedform orientations, bar morphology, and vegetation patterns help corroborate modeling results.

3.1. Tidal range effects on inlet velocities

Peak flood and ebb current velocities for each tidal cycle as recorded by the ADCP instrument located inside the inlet (Fig. 2A) are plotted against tidal range (TR) (Fig. 5). The R^2 values between TR and peak flood and ebb velocities are 0.64 and 0.74 (p-values <0.001), respectively, indicating a reasonable correspondence and sufficient evidence that the lines are significantly different (Moriasi et al., 2007). Additional statistical analyses substantiating this premise are presented in section-1 in SI. The regression lines reveal that during lower tidal ranges, ebb currents are stronger than the flood, but for TR $>\sim$0.7 m, flood currents increasingly dominate (Fig. 5). Because bedload sediment transport is related to the cube or higher order of velocity (Bagnold, 1966; Wang, 2011), as the system becomes more energetic due to increasing tidal range or during a storm surge, there is an increasingly greater influx of sand through the inlet and into the backbarrier tidal channels and the pond region. This tendency will lead to a gradual filling of the backbarrier that will help offset rising sea level and aid marsh resiliency.

3.2. Spatio-temporal hydrodynamics under different weather conditions

3.2.1. Comparison of normal tidal condition and November 2022 extratropical storm

Hydrodynamics at Allens Pond Inlet and backbarrier are analyzed by comparing modeled water levels and current velocities at the inlet channel to those within the pond region for three conditions: 1. Normal tidal condition, 2. Moderate southwest extratropical storm (November 2022), and 3. Hurricane Bob 1991 (Figs. 6–9). Water levels for normal tides and during the November extratropical 2022 storm exhibit similar trends of diminished tidal range and a substantial lag time at low tide at the inlet compared to the pond (Fig. 6). Under normal tidal conditions, the lower high tide elevation and smaller tidal range in the pond result from frictional resistance imparted to the landward propagating tidal wave across shallow meandering channels and around numerous sand bars (see Dronkers, 1986a,b). The average modeled tidal range at the inlet under normal tidal conditions is 0.61 m (measured = 0.66 m) and 0.40 m in the pond (measured = 0.48), indicating tidal dampening of 0.21 m (measure = 0.18 m) for mean tidal conditions (Fig. 6A). Most of the difference is attributed to the channel achieving a lower tidal elevation than that of the pond. The phase lag between the two sites is 1 h at high tide increasing to 2.6 h at low tide, which is explained by channel shoaling and increasing flow resistance. During the 16 November 2022 modeled storm, peak highwater in the inlet channel and pond occurred almost simultaneously with <5 cm difference in elevation. The subsequent low tide at the inlet channel dropped 20 cm lower than in the pond, which occurred 2.3 h later (Fig. 6B).

Modeled tidal currents in the inlet channel exhibit time asymmetry with the strongest flood currents occurring near high tide, whereas the highest ebb velocities occurred at mid-tide. The average peak ebb and flood velocities were almost equal (~41 cm/s; Fig. 7A). During the moderate extratropical storm during 16-17 November 2022, the peak flood and ebb currents were almost similar (~0.8 m/s; Fig. 7B) which were almost double compared to the average normal tide condition.

3.2.2. Hurricane Bob hydrodynamics and morphological impacts

As reported by Cheung et al. (2007), Hurricane Bob in 1991 produced a surge of >3 m causing widespread beach erosion, overwash, and severe damage to dwellings and infrastructure throughout Rhode Island and southern Massachusetts. Modeled maximum water levels at the inlet channel and in the pond occur almost simultaneously achieving the same elevation because the storm surge overtopped the barrier and filled

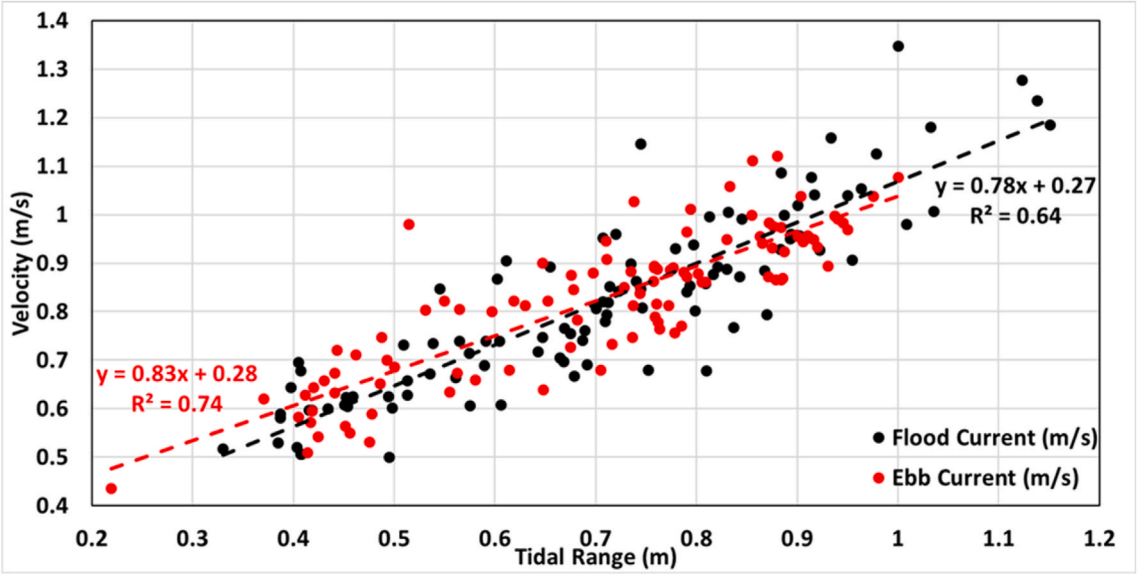

Fig. 5. Plot of tidal range versus maximum ebb and flood current velocities using data from ADCP located in the inlet channel (see Fig. 2A).

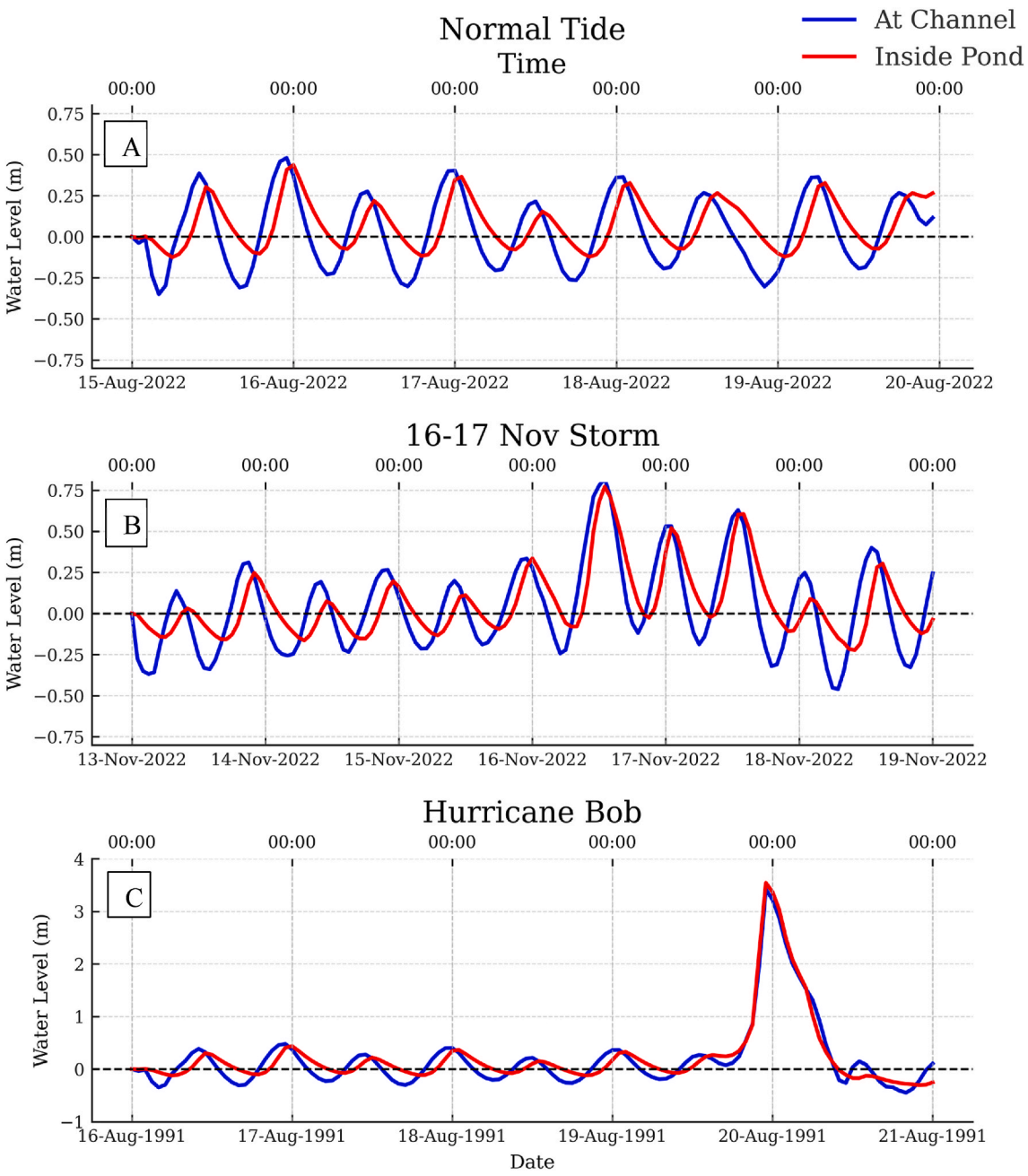

Fig. 6. Water levels at the inlet channel and within the pond during (A) normal tidal condition (B) 16-17 November 2022 extratropical storm, and (C) Hurricane Bob 1991. Note that the tide is substantially dampened as it propagates into the pond producing a high tide phase lag of ~1 h and low tide lag of ~1.5 h during (A) normal tide and (B) extratropical storm in November 2022.

the pond quickly (Fig. 6C and 8). Peak currents in the inlet channel were landward oriented, attaining 2.0 m/s early during the rising tide, diminishing to 1.5 m/s late during the ebb phase (Fig. 7C). The velocity asymmetry is explained by a steeper rising limb of the surge compared to falling limb leading to a shorter flood than ebb duration, the specifics of which are discussed below. Flow vectors and attendant water elevations chronicle the behavior of the storm in Fig. 8. The overall hydraulics of the system during the hurricane is related to the topography of the region, as shown in a longitudinal profile taken along the length of the barrier fronting Allens Pond (Fig. 9). It reveals a canal cut near the inlet and several low areas without high dunes or elevated gravel ridges that extend ~350 m west of the inlet and along the entire region landward of the eastern spit (Fig. 9). One hour prior to the peak storm surge, the model shows strong landward flow into the backbarrier from east and west of the inlet (Fig. 8A). This flow pattern was forced by rising water level in the coastal ocean (2.5 m above MLW) and a corresponding lower tide level (~2.0 m) in the backbarrier. As the storm tide heightened, the building surge poured through the inlet and across the marsh (Fig. 8A) accounting for peak waters levels to occur almost simultaneously in the coastal ocean and backbarrier region (6C and 8D). During maximum surge, flow vectors indicate that tidal waters overtopped most of western fronting barrier (Fig. 8C). The addition of this water produced a clockwise gyre in the backbarrier causing tidal waters to empty back through the inlet region (Fig. 8C). Shortly after this stage, the surge subsides (Fig. 8F) in the coastal ocean and currents continue to flow out the inlet (Fig. 8E). During both episodes of landward and seaward flowing currents, the barrier was eroded and largely flattened in elevation by 0 to >1.5 m (Fig. 9). During the same time, numerous surge channels and

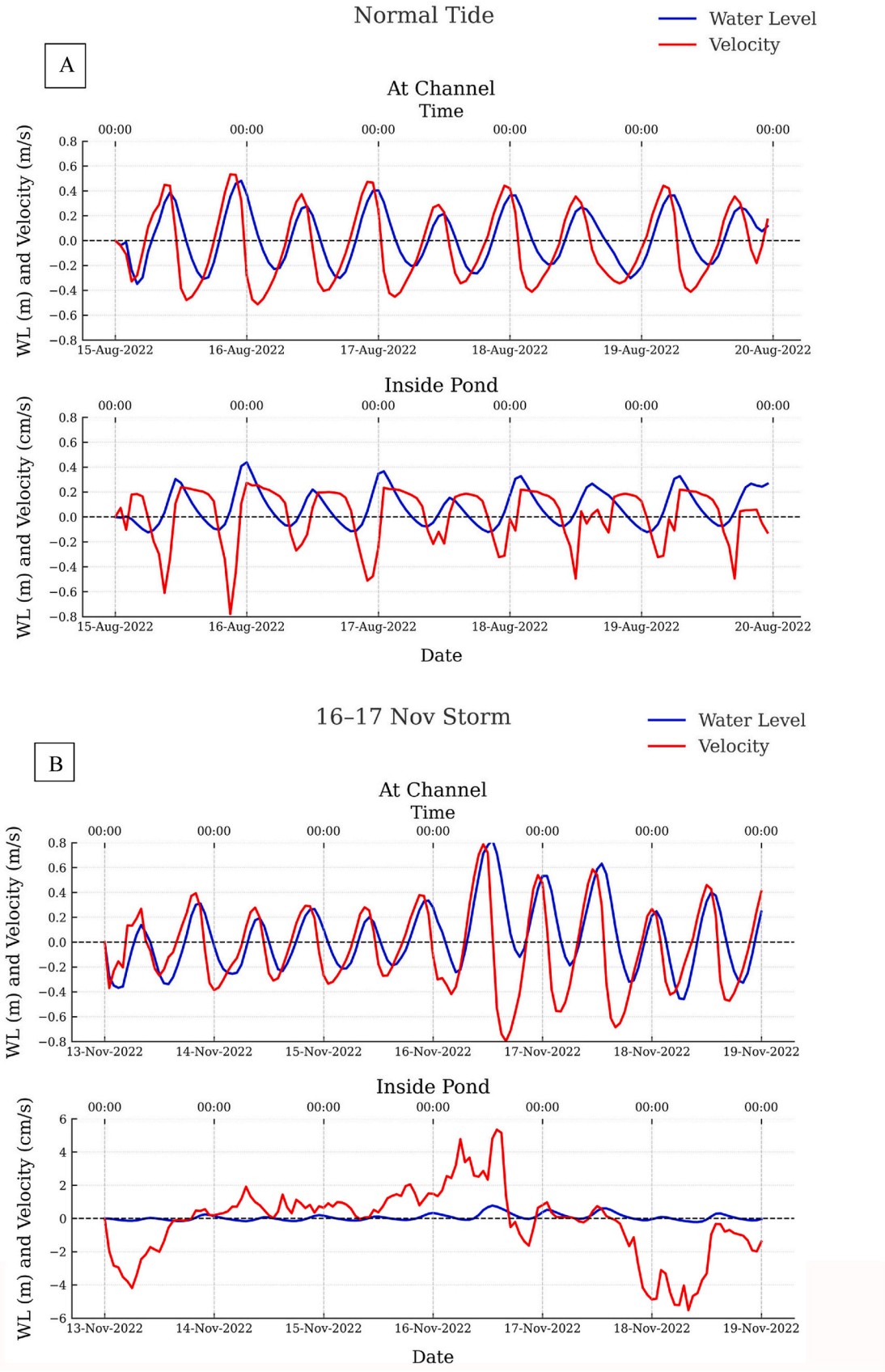

Fig. 7. Water Level and Velocity time series plot for both inlet channel and inside pond locations during (A) normal tide, (B) 16-17 November 2022 extratropical storm, and (C) Hurricane Bob 1991.

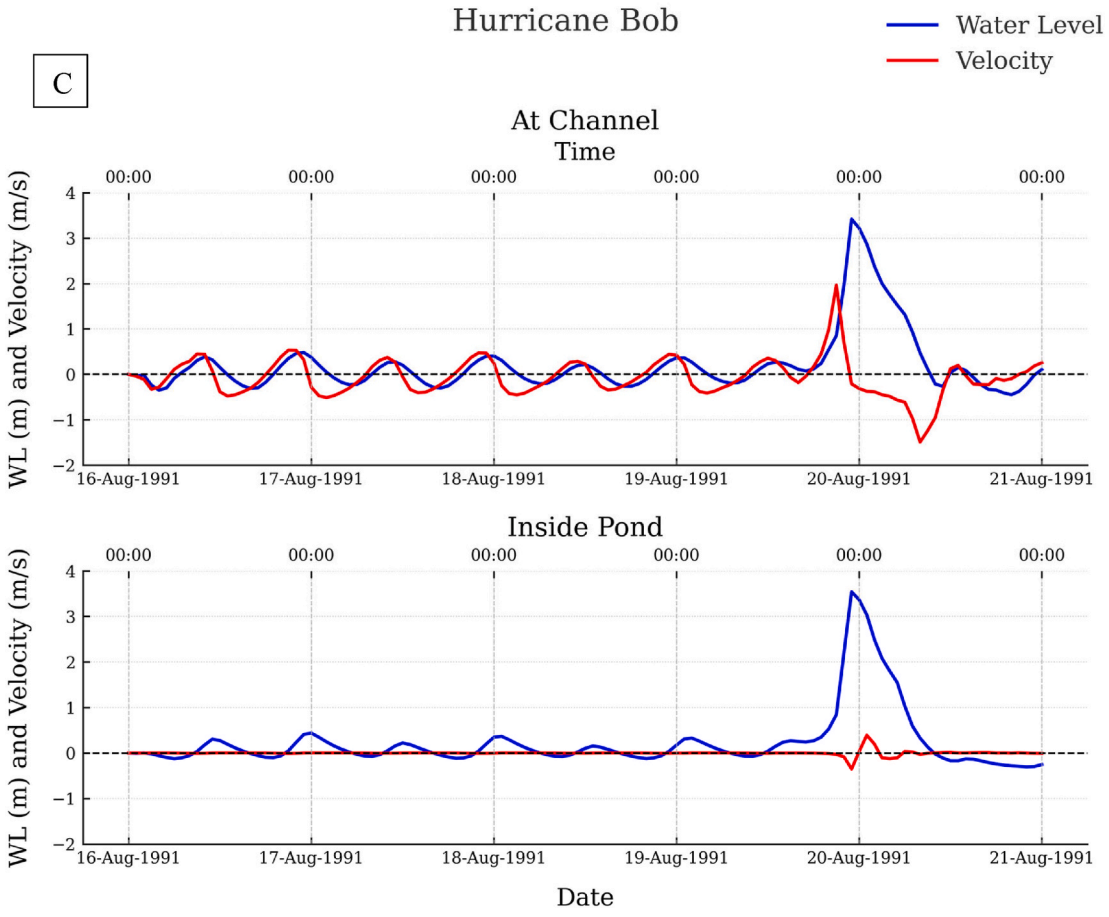

Fig. 7. (*continued*).

washover fans formed along the backside of the barrier, the scars of which are still evident along the backside of the barrier (see Fig. S2).

3.3. Spatial variations in sediment transport under different storm conditions

As shown in Fig. 8, the large storm surge that accompanied Hurricane Bob overtopped the eastern and western spits and sent tidal waters into Allens Pond and throughout backbarrier. Moreover, as the hurricane tracked northward and onshore winds reversed direction and began blowing offshore, the elevated tidal waters streamed back toward Buzzards Bay. During both episodes of landward and seaward flowing currents, the barrier was eroded and largely flattened by 0 to >1.5 m (Fig. 9). During the same time, numerous surge channels and washover fans formed along the backside of the barrier, the scars of which are still evident along the backside of the barrier (Fig. S2 in SI). The model-generated cumulative erosion and deposition during, before, and after Hurricane Bob are shown in Fig. 10.

Net sediment transport trends were studied using eight transects positioned across channels at the inlet mouth (T1) to six locations extending deeply into the backbarrier (T2, T3, T4, T5, T6, and T7), and finally at the entrance to the western pond (T8) (Fig. 3). Sediment fluxes were calculated for a 24-h period for normal tide (Fig. 11A), moderate storm (November 2022 extratropical storm) (Fig. 11B), and extreme storm (Hurricane Bob, 1991) conditions (Fig. 11C).

During normal tides, sediment influx into the pond from the ocean through the T1 is 8 m^3/day, and the sediment outflux from the pond to the ocean is 4 m^3/day (Fig. 11A). So, the net sediment flux is 4 m^3/day, importing sediment from the ocean to the pond (Fig. 11A). On the other hand, during a moderate storm, i.e., November 2022 extratropical storm, the sediment influx through the T1 from the ocean to the pond is 50 m^3/day, and the sediment outflux from the pond to the ocean is 40 m^3/day. So, the net sediment flux is almost 10 m^3/day, importing sediment from the ocean to the pond (Fig. 11B). Moreover, during an extreme event, (e.g., Hurricane Bob, 1991), the sediment influx through the T1 from the ocean to the pond is 1 560 m^3/day, and the sediment outflux from the pond to the ocean is 1 365 m^3/day. So, the net sediment flux is almost 195 m^3/day, importing sediment from the ocean to the pond (Fig. 11C).

Looking at transects T2-T8, located along the inlet channel to the pond (Fig. 3), we see that for normal tidal conditions as well as during the November 2022 moderate storm, net sediment flux, either influx or outflux, is very negligible (Fig. 11A and B). However, during the extreme event, Hurricane Bob 1991, notable volumes of sediment moved through the inlet and in the nearby channel (Fig. 11C; Transects 1-3, Fig. 3) in a net landward transport. Beyond T3, there was little transport.

The model results show that this microtidal pond system only gets significant volume of sediments during moderate to high-energy storms. Our results have shown that a major event like Hurricane Bob in 1991 could transport more than 20 times volume of sediments to this pond system from the ocean compared to a moderate event like the November 2022 extratropical storm. However, it should be acknowledged that between the occurrence of significant storms, such as Hurricane Bob, the cumulative effect of many moderate storms may be comparable.

3.4. Sediment distribution and morphology features in Allens Pond backbarrier

Our modeled sediment transport trends are largely corroborated by field data consisting of 31 sediment samples and measurements of

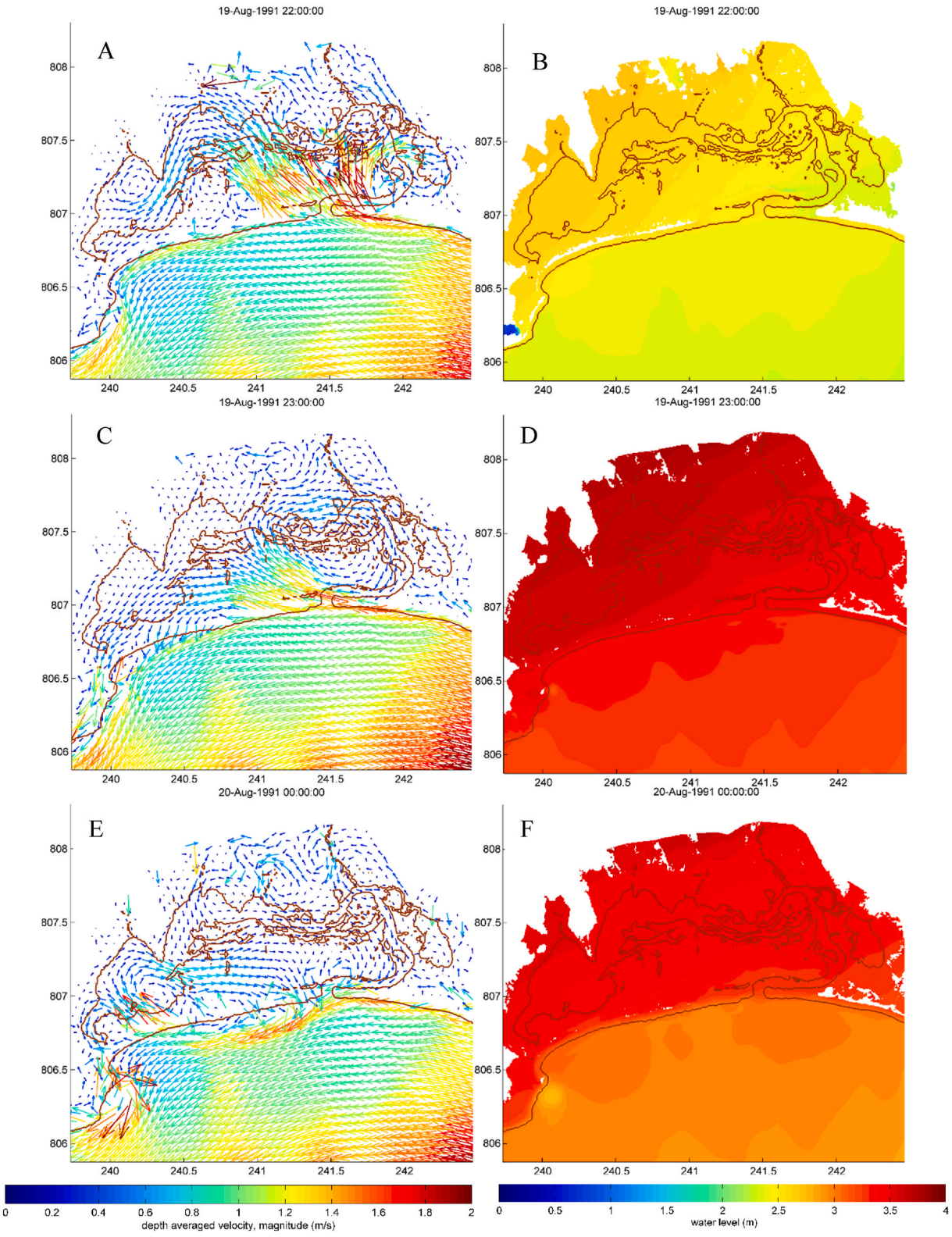

Fig. 8. Modeled flow vectors and water levels during 1991 Hurricane Bob for three periods: 1 h before peak surge (A & B), peak surge (C & D), and 1 h after peak surge (E & F).

bedform and intertidal shoal slipface orientations (see section 2.2 for details of data collection). The backbarrier channels and shoals consist of medium to fine sand exhibiting considerable variability because some samples were collected in energetic tidal channels whereas others were taken on protected intertidal shoals. Despite the variability, there is an overall pattern ranging from ~0.5 to 2.0 phi (Φ) at the mouth and inlet channel to 2.0 to 2.5 phi in the mid-backbarrier region to 2.5 to 3.0 at the entrance to the pond (Fig. 12). The general trend of landward fining in grain size suggests a net landward transport of sand, which is consistent with the overall hydraulic regime of dominant flood currents,

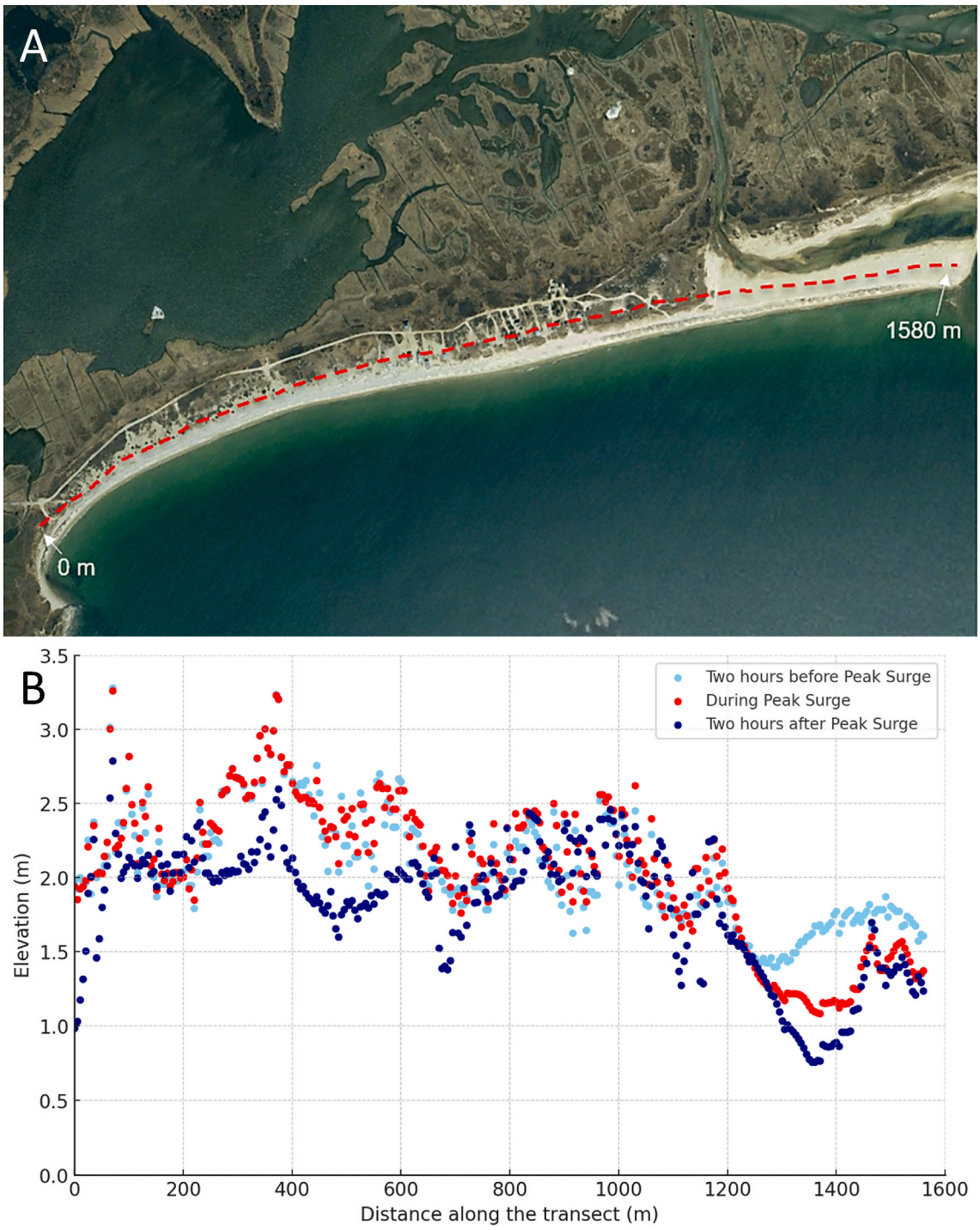

Fig. 9. Topographic longitudinal transect along barriers fronting Allens Pond backbarrier. (A) Location of transect. (B) Initial elevations determined from Lidar. Note that in most locations, the pre-surge overtopping of the barrier (light blue dots) sit at a higher elevation than after seaward and landward flow across the barrier. Sites that experienced apparent accretion are attributed to washover deposition. (For interpretation of the references to colour in this figure legend, the reader is referred to the Web version of this article.)

landward-oriented intertidal bedforms, and existence of numerous flood-tidal deltas (Fig. 13). Fig. 13 also depicts an arcuate shoal that is prograding into the pond, indicating net landward movement of sediment. A final suggestion that the backbarrier is receiving sand is the fact that shoals are accreting vertically at a high enough rate such that numerous sites are being colonized by pioneering stands of short-form *Spartina*, despite a sea-level rise rate in this region approximating 3.13 mm/yr at Woods Hole, MA (NOAA, 2025).

4. Discussion

4.1. Comparison to other inlets

This study highlights the significant role that major storms impose on the sediment transport trends of small tidal inlets (width <100 m), using the Allens Pond backbarrier and inlet system along the microtidal coast of Buzzards Bay, Massachusetts, as an example. While typically, these events are short in duration, the hydrodynamic characteristics of these

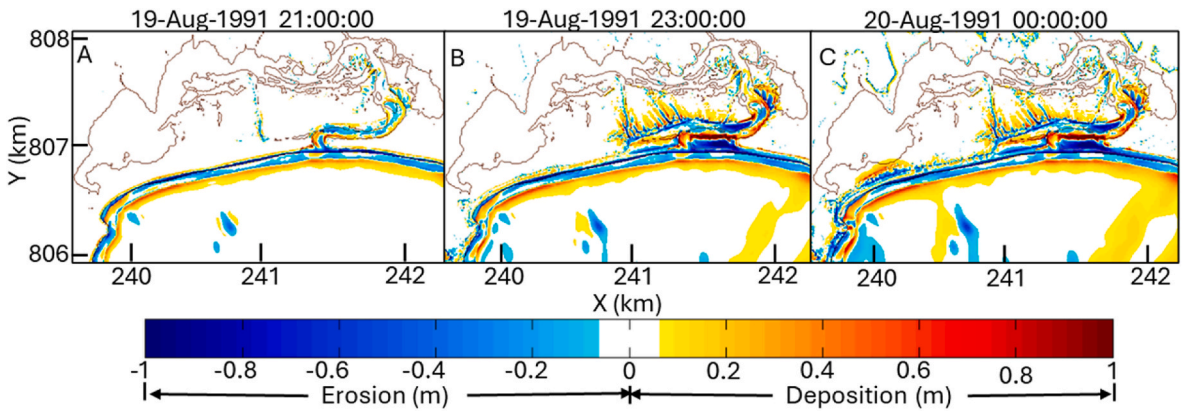

Fig. 10. Cumulative Erosion-Deposition for Allens Pond region for various periods during the 1991 Hurricane Bob: (A) 2 h before peak surge, (B) at peak surge, and (C) 1 h after peak surge. Generally, the storm eroded the beach and transported sediment to the nearshore. Additionally, the eastern spit was eroded, and much of this sand was moved into the main inlet channel and into the eastern portion of the backbarrier. Along the shore, west of the inlet, sand was transported onto the marsh while the beach and dunes were eroded and flattened.

storms produce a consistent pattern of erosion and deposition and long-term trends in net sediment transport. Our results provide valuable insights into the sediment dynamics of small estuarine/inlet systems, particularly considering the predicted climate change-induced intensification of storms. Using a combination of numerical modeling, field observations, and sedimentological analysis, we have demonstrated that hurricanes, and by inference large magnitude extra-tropical cyclones, control sediment transport, deposition, and backbarrier infilling processes.

Unlike larger tidal inlets (width >100 m), storm-generated sediment transport at small inlets is primarily boosted by the storm surge that creates a steep water surface slope extending from the coastal ocean into the inlet channel thereby generating strong flood currents and landward sediment transport. This situation contrasts with larger-sized inlets where, in addition to effects of the storm surge, shoaling and breaking waves enhance storm surge flow, as demonstrated in a modeling study by (Irish et al., 2009). Likewise, hydrodynamics modeling of Texel Inlet in The Netherlands, revealed that wind and waves augment flood-tidal currents increasing sediment transport into the basin (Elias et al., 2006). Finally, numerical simulations of hydraulics and sediment transport during Hurricane Sandy corroborated that flood currents move marine sediment into Jamaica Bay (Wang et al., 2017).

One of the major findings of this study is that under normal tidal conditions the system experiences a moderate net import of sand (Fig. 10A). Storm events substantially amplify this transport signal, enhancing sediment influx through the inlet and into the backbarrier by more than an order of magnitude (~20x) (Fig. 10B and C). These results highlight the dominant role of energetic hydrodynamic forcing in controlling sediment exchange at small inlet systems. Similar processes were used to explain the growth of flood deltas and sand shoals inside Ninigret Inlet (width <100 m) on the Rhode Island by Boothroyd et al. (1985). These results contrast with a study by Castagno et al. (2018) who evaluated the effects of various storm parameters at Virginia tidal inlets using hydrodynamic and sediment-transport simulations. They found that increasing storm magnitude and duration caused greater import of mud and fine sand into the backbarrier whereas coarser sand fractions were exported. The differences in our findings might be explained by scale, as Virginia inlets are all large systems and Allens Pond Inlet is small. In addition, the muddy nearshore of the Virginia coast (Fenster et al., 2016) contrasts with the sandy nature offshore of Allens Pond (Xie et al., 2024b).

Field observations and sediment grain-size analysis support our model predictions. The gradual fining of sediment from the spit and inlet through the tidal channels and into the pond indicates net landward sand transport (Fig. 12). The presence of flood-oriented bedforms and point bars further supports the hypothesis that storm-driven hydrodynamics enhance net landward sediment flux (Fig. 13). The colonization of the flood shoals by *Spartina alterniflora* (Fig. 13) provides additional evidence of long-term sediment deposition and vertical accretion. Since *Spartina alterniflora* establishes only on surfaces that are at or above mean sea level, its presence on sand shoals suggests ongoing elevation gains driven by sediment deposition is sufficient to overcome a regime of accelerating sea-level rise (Schuerch et al., 2013).

4.2. Implications for coastal morphodynamics and management

The study underscores the importance of storm processes in regulating sediment budgets in microtidal and small inlets/estuaries. Unlike mesotidal systems, where tidal currents dominate sediment transport (Georgiou et al., 2024), small inlets are more susceptible to external forcings, particularly from wave action and storm surges. Our results demonstrate that in the absence of significant tidal forcing, storm events act as primary drivers of sediment exchange between the coastal ocean and backbarrier environments (Fig. 11C). This has significant implications for predicting how these systems will respond to future climatic changes.

One of the most pressing concerns for coastal managers is how estuarine and backbarrier environments will adapt to rising sea levels (FitzGerald et al., 2007; Hein et al., 2021). Our findings indicate that storm-driven sediment deposition may help counteract the effects of relative sea-level rise in small tidal inlets. As storm frequency and intensity increase under climate change scenarios (Pang et al., 2023), it is possible that increased sediment fluxes may partially offset submergence by promoting vertical accretion of tidal flats and marshes (Cahoon et al., 2000).

However, this process is conditional on the continued availability of sediment sources. If sediment supply becomes limited due to anthropogenic modifications such as dredging, shoreline stabilization, or coastal armoring, the ability of these systems to naturally adapt to sea-level rise may be compromised (Griggs and Reguero, 2021). Additionally, while storm-induced deposition can contribute to vertical accretion, it can also lead to unintended consequences such as inlet closure or excessive shoaling (Rodriguez et al., 2020), which may alter hydrodynamic connectivity between the ocean and the backbarrier system.

As climate change continues to reshape coastal dynamics, understanding the role of storm-driven sediment transport will be critical for predicting how barrier systems will evolve (Anarde et al., 2024). While storm events can pose immediate hazards, they also provide an essential mechanism for sediment redistribution, which may support the resilience of backbarrier environments (Georgiou et al., 2024).

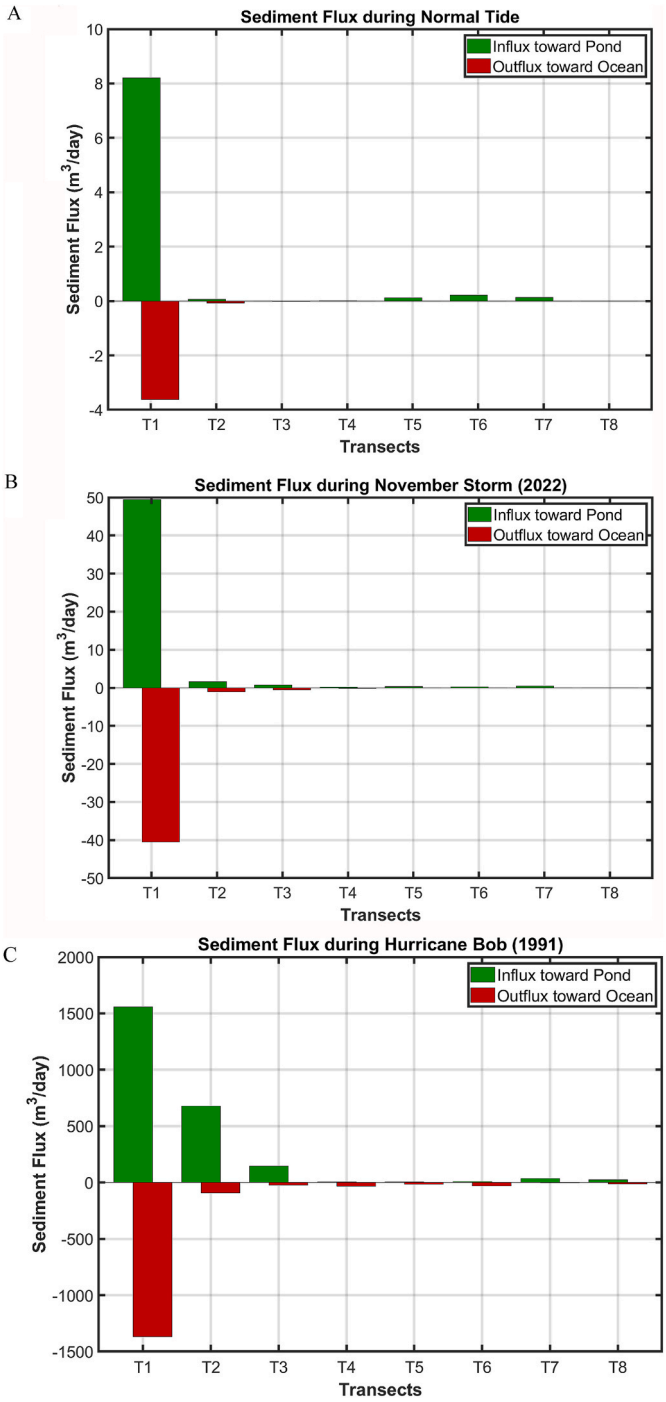

Fig. 11. Sediment flux in m^3 per day period for transects T1-T8 (see Fig. 2) during (A) normal tide, (B) Extratropical storm in November 2022, and (C) Hurricane Bob in 1991.

This research combines field data, numerical modeling, and ecological indicators, thereby offering a comprehensive framework for assessing storm-induced sediment transport at small tidal inlet systems. Future research should explore interactions among extreme weather events, sediment budgets, and ecosystem stability, particularly in regions where sediment supply is constrained.

4.3. Limitations to this study

Although we made substantial efforts to replicate this complex small inlet backbarrier system within the numerical model, several limitations remain. First, we represented the channel bed and shoals using a single grain size. This decision was guided by the primary objective of the study to quantify the transport of sand within the Allens Pond system, which was established from sediment samples collected during this study as well as from sample gathered throughout the region (Xie et al., 2024b). Nevertheless, this simplification does not account for the full range of sediment heterogeneity that may influence transport dynamics under varying hydrodynamic conditions. For example, adopting a smaller representative grain size would reduce settling velocity and the critical shear stress for motion, which would generally increase predicted suspended concentrations and sediment fluxes; conversely, using a coarser grain size would increase entrainment thresholds and settling rates, thereby reducing transport magnitudes (Ferguson and Church, 2004). Meanwhile, a multi-fraction sediment formulation can better represent spatial sorting and condition-dependent transport pathways in barrier island inlet systems (e.g., Herrling and Winter, 2014). Therefore, our single sediment grain size setup may bias the absolute flux magnitudes and the partitioning between bedload and suspended load. However, given the much stronger hydrodynamic forcing during storms relative to normal tidal conditions, our main conclusion regarding storm-dominated sediment exchange is qualitatively robust (Georgiou et al., 2024).

The second limitation of this study is the lack of direct validation of modeled sediment fluxes, although the hydrodynamics were validated against observed water levels and velocities (Fig. 4). Direct validation of sediment transport was not feasible because transport in this system is predominantly bedload, and reliable bedload/total sediment flux measurements in energetic inlet environments, particularly during storms, are difficult to obtain in practice (Hubbell, 1964; Ernstsen et al., 2008). Accordingly, we evaluated transport predictions using independent sedimentologic and geomorphic evidence (Figs. 12 and 13) to corroborate modeled transport pathways and depositional patterns, consistent with recommended approaches for coastal sediment transport modeling when direct flux observations are unavailable (Williams and Esteves, 2017; Willmott, 1981).

Finally, the absence of velocity measurements within the pond represented another limitation of this study. The instrument deployed at that location was a water level logger, which provided reliable stage data but did not record current velocities. As a result, we were unable to directly validate modeled flow velocities within the pond basin. This constraint introduces additional uncertainty in assessing circulation patterns and sediment transport processes in that portion of the system. Future work should include more systematic field measurements of water levels and currents within the pond and at the inlet, which are widely recommended for robust calibration and validation of coastal hydrodynamic and sediment-transport models (Williams and Esteves, 2017).

5. Conclusions

This study provides critical insights into the sediment dynamics and morphological evolution of Allens Pond Inlet, a small microtidal system in Buzzards Bay, Massachusetts. By combining numerical modeling, field observations, and sedimentological analysis, we have demonstrated that storm events play a dominant role in controlling sediment transport and back-barrier infilling processes. Under normal tidal conditions, the system exhibits a slight net import of sediment, although the associated volume is small. In contrast, storm events - particularly those of moderate to extreme intensity - drive substantial sediment influx into the pond. Extreme storms, such as Hurricane Bob in 1991, transport sediment volumes that are orders of magnitude larger than those observed during moderate storms, highlighting the importance of storm-driven processes in shaping the long-term geomorphic evolution of microtidal inlets. Additionally, the storm surge from large hurricanes (e.g., Hurricane Bob) can overtop the adjacent barriers overwashing sediment into the backbarrier.

Fig. 12. Fining mean grain size (Φ) trend suggests a new landward transport of sediment through the inlet and into the back barrier.

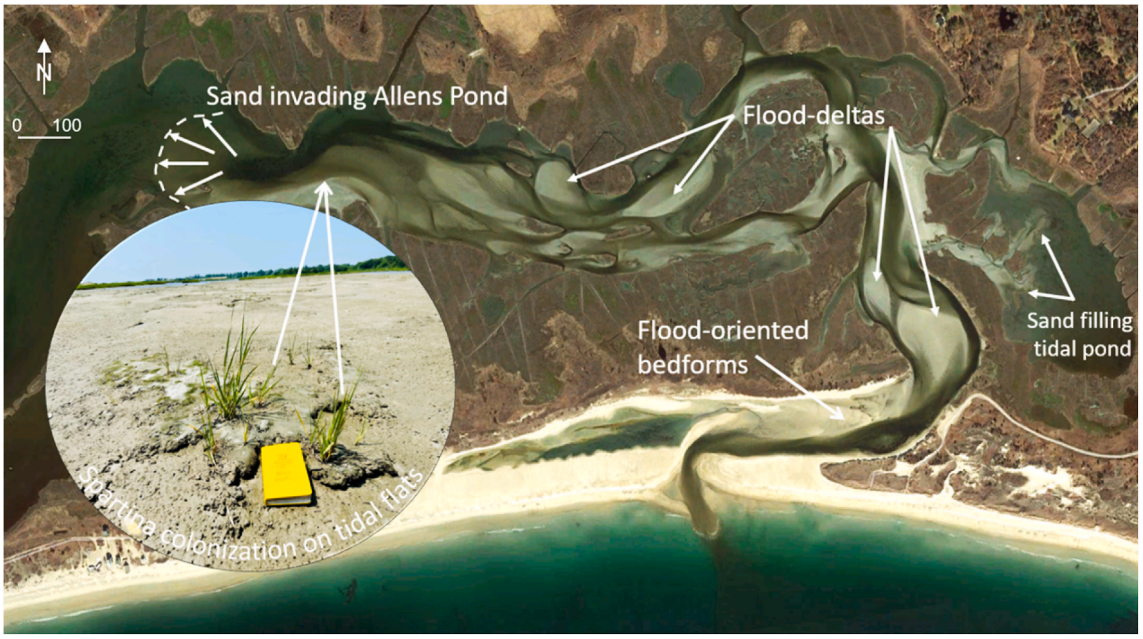

Fig. 13. Flood oriented bedforms and bar morphology indicate landward sand transport. Circled image, captured by the author, shows where *Spartina* is colonizing on tidal flats.

The progressive fining of sediment grain size from the spit through the channel and into the pond, along with the presence of flood-oriented bedforms and *Spartina alterniflora* colonization, provides strong evidence of landward sediment transport and deposition. These findings underscore the sensitivity of microtidal inlets to external forcing, particularly from storm waves and surges, which act as primary drivers of sediment delivery to the inlet and exchange between the coastal ocean and backbarrier environments.

From a management perspective, this study highlights the need to consider storm dynamics when designing strategies for maintenance and ecological conservation at small inlets. While storm-driven sediment deposition can enhance the resilience of backbarrier environments by promoting vertical accretion and offsetting the impacts of sea level rise, it also poses challenges such as potential inlet closure and excessive shoaling. Balancing these competing factors will require an integrated approach that prioritizes the preservation of natural sediment sources and minimizes anthropogenic disruptions to sediment transport pathways.

In conclusion, this study advances our understanding of storm-driven sediment transport processes at small tidal inlets and provides a valuable foundation for future research aimed at improving the resilience of coastal environments in the face of an increasingly changing climate. Continued monitoring and adaptive management will be essential in the future to safeguarding these dynamic and important coastal landscapes.

CRediT authorship contribution statement

Tansir Zaman Asik: Conceptualization, Data curation, Formal analysis, Investigation, Methodology, Validation, Visualization, Writing – original draft. **Duncan FitzGerald:** Conceptualization, Funding acquisition, Investigation, Methodology, Project administration, Resources, Supervision, Writing – review & editing. **Danghan Xie:** Data curation, Formal analysis, Methodology, Validation, Visualization, Writing – review & editing. **Ioannis Y. Georgiou:** Methodology, Resources, Validation, Visualization, Writing – review & editing. **Zoe Hughes:** Conceptualization, Funding acquisition, Project administration, Software. **Silke Tas:** Data curation, Methodology.

Declaration of competing interest

The authors declare that they have no known competing financial interests or personal relationships that could have appeared to influence the work reported in this paper.

Acknowledgments

This research is funded by the Buzzards Bay Coalition through a grant from The Rathmann Family Foundation with additional support from Mass Audubon, Allens Pond Wildlife Sanctuary. We would like to thank Sarah Black, Sophia Tigges, Matt Giese, Abbi Sloot, Ellie Bortman, Brooke Tillotson, Simone Fishman, Evie Usich and Rebecca Rudolph for their assistance collecting and analyzing field measurements.

Appendix A. Supplementary data

Supplementary data to this article can be found online at https://doi.org/10.1016/j.coastaleng.2026.105075.

Data availability

The wave data are collected from an offshore buoy station (Station No.: BUZM3 & 44085) maintained by the National Data Buoy Center (NDBC, 2025). The historical tidal level for the regional model is retrieved from the Newport tidal gauge (Station No.: 8452660) operated by NOAA (NOAA, 2025). Storm surge, peak wave height and wave direction of historical storm events are obtained from a regional modeling data set by the NACCS Coastal Hazards System (Cialone et al., 2015). Delft3D is an open-source code available online (Deltares, 2014).

References

Amante, C.J., Love, M., Carignan, K., Sutherland, M.G., MacFerrin, M., Lim, E., 2023. Continuously updated digital elevation models (CUDEMs) to support coastal inundation modeling. Remote Sens. 15 (6), 1702. https://doi.org/10.3390/rs15061702.

Anarde, K.A., Moore, L.J., Murray, A.B., Reeves, I.R., 2024. The future of developed barrier systems: 1. Pathways toward uninhabitability, drowning, and rebound. Earths Future 12 (4). https://doi.org/10.1029/2023EF003672 e2023EF003672.

Avilés, L.B., 2014. Fire Island past, present, and future: the environmental history of a barrier beach. Environ. Hist. 19 (2), 375–377. April 2014, Published by: Oxford University Press on behalf of Forest History Society and American Society for Environmental History. https://www.jstor.org/stable/24690576.

Bagnold, R.A., 1966. An Approach to the Sediment Transport Problem from General Physics. US government printing office.

Baranes, H., Dykstra, S.L., Jay, D.A., Talke, S.A., 2023. Sea level rise and the drivers of daily water levels in the Sacramento-San Joaquin Delta. Sci. Rep. 13 (1), 22454. https://doi.org/10.1038/s41598-023-49204-z.

Barwis, J.H., 1976. Annotated bibliography on the geologic, hydraulic, and engineering aspects of tidal inlets. In: US Army Engineer Waterways Experiment Station, vol. 4.

Booij, N., Ris, R.C., Holthuijsen, L.H., 1999. A third-generation wave model for coastal regions: 1. Model description and validation. J. Geophys. Res. 104 (C4), 7649–7666. https://doi.org/10.1029/98jc02622.

Boon III, J.D., Byrne, R.J., 1981. On basin hyposmetry and the morphodynamic response of coastal inlet systems. Mar. Geol. 40 (1–2), 27–48. https://doi.org/10.1016/0025-3227(81)90041-4.

Boothroyd, J.C., Friedrich, N.E., McGinn, S.R., 1985. Geology of microtidal coastal lagoons: rhode Island. Mar. Geol. 63 (1–4), 35–76. https://doi.org/10.1016/0025-3227(85)90079-9.

Cahoon, D.R., Marin, P.E., Black, B.K., Lynch, J.C., 2000. A method for measuring vertical accretion, elevation, and compaction of soft, shallow-water sediments. J. Sediment. Res. 70 (5), 1250–1253. https://doi.org/10.1306/020800701250.

Castagno, K.A., Jiménez-Robles, A.M., Donnelly, J.P., Wiberg, P.L., Fenster, M.S., Fagherazzi, S., 2018. Intense storms increase the stability of tidal bays. Geophys. Res. Lett. 45 (11), 5491–5500. https://doi.org/10.1029/2018GL078208.

Chan, M.C., 2023. Sizing a small tidal inlet for restoration. J. Coast Res. 39 (4), 610–624. https://doi.org/10.2112/JCOASTRES-D-22-00103.1.

Cheung, K.F., Tang, L., Donnelly, J.P., Scileppi, E.M., Liu, K.B., Mao, X.Z., et al., 2007. Numerical modeling and field evidence of coastal overwash in southern New England from Hurricane Bob and implications for paleotempestology. J. Geophys. Res. 112 (F3). https://doi.org/10.1029/2006jf000612.

Cialone, M.A., Massey, T.C., Anderson, M.E., Grzegorzewski, A.S., Jensen, R.E., Cialone, A., et al., 2015. North Atlantic Coast Comprehensive Study (NACCS) coastal storm model simulations: waves and water levels. https://chs.erdc.dren.mil/Home [Coastal Hazards System].

CIRES, 2014. Continuously Updated Digital Elevation Model (CUDEM) - 1/9 ArcSecond resolution bathymetric-topographic tiles. Tiles 41. https://doi.org/10.25921/ds9vky35, 25-41.50N, 71.00-71.25W. NOAA National Centers for Environmental Information.

Deltares, 2014. Simulation of multi-dimensional hydrodynamic flows and transport phenomena, including sediments - user manual. Deltares [Delft3D Software]. Retrieved from, Version: 3.15.34158. https://oss.deltares.nl/.

Dissanayake, D.M.P., Ranasinghe, R., Roelvink, J.A., 2012. The morphological response of large tidal inlet/basin systems to relative sea level rise. Clim. Change 113 (2), 253–276. https://doi.org/10.1007/s10584-012-0402-z.

Donnelly, J.P., Bryant, S.S., Butler, J., Dowling, J., Fan, L., Hausmann, N., et al., 2001. 700 yr sedimentary record of intense hurricane landfalls in southern New England. Geol. Soc. Am. Bull. 113 (6), 714–727. https://doi.org/10.1130/0016-7606(2001)113%3C0714:YSROIH%3E2.0.CO;2.

Dronkers, J., 1986a. Tidal asymmetry and estuarine morphology. Neth. J. Sea Res. 20 (2–3), 117–131. https://doi.org/10.1016/0077-7579(86)90036-0.

Dronkers, J., 1986b. Tide-induced residual transport of fine sediment. Phys. Shallow Estuar. Bays 16, 228–244. https://doi.org/10.1029/LN016p0228.

Duong, T.M., 2021. Climate change induced coastline change adjacent to small tidal inlets. Front. Mar. Sci. 8, 754756. https://doi.org/10.3389/fmars.2021.754756.

Duong, T.M., Ranasinghe, R., Luijendijk, A., Walstra, D., Roelvink, D., 2017. Assessing climate change impacts on the stability of small tidal inlets: part 1-Data poor environments. Mar. Geol. 390, 331–346. https://doi.org/10.1016/j.margeo.2017.05.008.

Elias, E.P.L., Cleveringa, J., Buijsman, M.C., Roelvink, J.A., Stive, M.J.F., 2006. Field and model data analysis of sand transport patterns in Texel Tidal inlet (the Netherlands). Coast. Eng. 53 (5–6), 505–529. https://doi.org/10.1016/j.coastaleng.2005.11.006.

Ernstsen, V.B., Becker, M., Winter, C., Bartholomä, A., Flemming, B.W., Bartholdy, J., 2008. Bedload transport in an inlet channel during a tidal cycle. River, Coastal and Estuarine Morphodynamics. RCEM 2007. Dohmen-Janssen & Hulscher, pp. 1–8 eds.

Fenster, M.S., Dolan, R., Smith, J.J., 2016. Grain-size distributions and coastal morphodynamics along the southern Maryland and Virginia barrier island. Sedimentolog 63 (4), 809–823. https://doi.org/10.1111/sed.12239.

Ferguson, R.I., Church, M., 2004. A simple universal equation for grain settling velocity. J. Sediment. Res. 74 (6), 933–937. https://doi.org/10.1306/051204740933.

FitzGerald, D.M., 1993. Origin and stability of tidal inlets in Massachusetts. Formati. Evol. Multiple Tidal Inlet. 44, 1–61. https://doi.org/10.1029/CE044p0001.

FitzGerald, D.M., 1996. Geomorphic variability and morphologic and sedimentologic controls on tidal inlets. J. Coast Res. 12 (1), 47–70. https://www.jstor.org/stable/25736068.

FitzGerald, D., Kulp, M., Hughes, Z., Georgiou, I., Miner, M., Penland, S., Howes, N., 2007. Impacts of rising sea level to backbarrier wetlands, tidal inlets, and barrier islands: barataria Coast, Louisiana. Coast. Sediments' 07 1179–1192. https://doi.org/10.1061/40926(239)91.

FitzGerald, D.M., Baldwin, C.T., Ibrahim, N.A., Humphries, S.M., 1992. Sedimentologic and Morphologic Evolution of a Beach Ridge Barrier Along an Indented Coast: Buzzards Bay, Massachusetts. https://doi.org/10.2110/pec.92.48.0065.

FitzGerald, D.M., Baldwin, C.T., Ibrahim, N.A., Sands, D.R., 1987. Development of the northwestern Buzzards Bay shoreline, Massachusetts. In: Glaciated Coasts. Academic Press, Inc., pp. 327–357, 18 fig, 38 ref.

FitzGerald, D.M., Buynevich, I., Argow, B., 2006. Model of tidal inlet and barrier island dynamics in a regime of accelerated sea level rise. J. Coast Res. 789–795. https://www.jstor.org/stable/25741684.

FitzGerald, D.M., Hughes, Z.J., Staro, A., Hein, C.J., Sakib, M.M., Georgiou, I.Y., Novak, A., 2022. Following the sand grains. J. Mar. Sci. Eng. 10, 631. https://doi.org/10.3390/jmse1005063.

FitzGerald, D.M., Van Heteren, S., 1999. Classification of paraglacial barrier systems: coastal New England, USA. Sedimentology 46 (6), 1083–1108. https://doi.org/10.1046/j.1365-3091.1999.00266.x.

Folk, R.L., Ward, W.C., 1957. Brazos River bar [Texas]; a study in the significance of grain size parameters. J. Sediment. Res. 27 (1), 3–26. https://doi.org/10.1306/74D70646-2B21-11D7-8648000102C1865D.

Friedrichs, C.T., Aubrey, D.G., 1988. Non-linear tidal distortion in shallow well-mixed estuaries: a synthesis. Estuar. Coast Shelf Sci. 27 (5), 521–545. https://doi.org/10.1016/0272-7714(88)90082-0.

Georgiou, I.Y., FitzGerald, D.M., Hanegan, K.C., 2024. Storm and tidal interactions control sediment exchange in mixed-energy coastal systems. PNAS Nexus 3 (2), 1–11. https://doi.org/10.1093/pnasnexus/pgae042.

Griggs, G., Reguero, B.G., 2021. Coastal adaptation to climate change and sea-level rise. Water 13 (16), 2151. https://doi.org/10.3390/w13162151.

Hanegan, K.C., FitzGerald, D.M., Georgiou, I.Y., Hughes, Z.J., 2023. Long-term sea level rise modeling of a basin-tidal inlet system reveals sediment sinks. Nat. Commun. 14 (1), 7117. https://doi.org/10.1038/s41467-023-42895-y.

Hayes, M.O., FitzGerald, D.M., 2013. Origin, evolution, and classification of tidal inlets. J. Coast. Res. SI 69, 14–33. https://doi.org/10.2112/SI_69_3.

Hein, C.J., Fenster, M.S., Gedan, K.B., Tabar, J.R., Hein, E.A., DeMunda, T., 2021. Leveraging the interdependencies between barrier islands and backbarrier saltmarshes to enhance resilience to sea-level rise. Front. Mar. Sci. 8, 721904. https://doi.org/10.3389/fmars.2021.721904.

Herrling, G., Winter, C., 2014. Morphological and sedimentological response of a mixed-energy barrier island tidal inlet to storm and fair-weather conditions. Earth Surf. Dyn. 2 (1), 363–382. https://doi.org/10.5194/esurf-2-363-2014.

Hubbell, D.W., 1964. Apparatus and techniques for measuring bedload. Geol. Survey Water Supply Paper 1748. United States Depart. Interior 80.

Irish, J.L., Resio, D.T., Cialone, M.A., 2009. A surge response function approach to coastal hazard assessment. Part 2: quantification of spatial attributes of response functions. Nat. Hazards 51 (1), 183–205. https://doi.org/10.1007/s11069-009-9381-4.

Knutson, T.R., Sirutis, J.J., Zhao, M., Tuleya, R.E., Bender, M., Vecchi, G.A., et al., 2015. Global projections of intense tropical cyclone activity for the late twenty-first century from dynamical downscaling of CMIP5/RCP4. 5 scenarios. J. Clim. 28 (18), 7203–7224. https://doi.org/10.1175/JCLI-D-15-0129.1.

Kossin, J.P., Knapp, K.R., Olander, T.L., Velden, C.S., 2020. Global increase in major tropical cyclone exceedance probability over the past four decades. Proc. Natl. Acad. Sci. 117 (22), 11975–11980. https://doi.org/10.1073/pnas.1920849117.

Lesser, G.R., Roelvink, J.A., van Kester, J.A.T.M., Stelling, G.S., 2004. Development and validation of a three-dimensional morphological model. Coast. Eng. 51 (8–9), 883–915. https://doi.org/10.1016/j.coastaleng.2004.07.014.

Mallinson, D.J., Culver, S.J., Riggs, S.R., Walsh, J.P., Ames, D., Smith, C.W., 2008. Past, Present, and Future Inlets of the Outer Banks Barrier Islands, North Carolina. East Carolina University. Department of Geological Sciences, Thomas Harriot College of Arts and Sciences, and Institute for Coastal Science and Policy. https://geology.ecu.edu/wp-content/pv-uploads/sites/196/2019/05/Inlets-Past-presentand-future.pdf.

Moriasi, D.N., Arnold, J.G., Van Liew, M.W., Bingner, R.L., Harmel, R.D., Veith, T.L., 2007. Model evaluation guidelines for systematic quantification of accuracy in watershed simulations. Trans. ASABE 50 (3), 885–900. https://doi.org/10.13031/2013.23153.

NDBC, 2025. Wind and wave data collected from National Data Buoy Center (station no.: BUZM3 & 44085). NDBC. Retrieved from. https://www.ndbc.noaa.gov/.

NOAA, 2025. Historical tidal level data retrieved from Newport tidal gauge under National Oceanic and Atmospheric Administration (Station No.:8452660). NOAA. https://tidesandcurrents.noaa.gov/.

OCM Partners, 2018. 2018 USACE NCMP topobathy lidar DEM: east Coast (CT, MA, ME, NC, NH, RI, SC). Retrieved 2023-02-03, from. https://www.fisheries.noaa.gov/inport/item/55882.

Pang, T., Wang, X., Nawaz, R.A., Keefe, G., Adekanmbi, T., 2023. Coastal erosion and climate change: a review on coastal-change process and modeling. Ambio 52 (12), 2034–2052. https://doi.org/10.1007/s13280-023-01901-9.

Rodriguez, A.B., Theuerkauf, E.J., Ridge, J.T., VanDusen, B.M., Fegley, S.R., 2020. Long-term washover fan accretion on a transgressive barrier island challenges the assumption that paleotempestites represent individual tropical cyclones. Sci. Rep. 10 (1), 19755. https://doi.org/10.1038/s41598-020-76521-4.

Schuerch, M., Vafeidis, A., Slawig, T., Temmerman, S., 2013. Modeling the influence of changing storm patterns on the ability of a salt marsh to keep pace with sea level rise. J. Geophys. Res. Earth Surf. 118 (1), 84–96. https://doi.org/10.1029/2012JF002471.

Senthilkumar, R., Murali, K., Sundar, V., 2017. Stability of micro-tidal inlets along coastlines dominated by Littoral drift. J. Coast Conserv. 21 (2), 283–292. https://doi.org/10.1007/s11852-017-0537-1.

Stutz, M.L., Pilkey, O.H., 2001. A review of global barrier island distribution. J. Coast Res. 15–22. https://www.jstor.org/stable/25736270.

Sun, Y., Chen, C., Beardsley, R.C., Xu, Q., Qi, J., Lin, H., 2013. Impact of current- wave interaction on storm surge simulation: a case study for hurricane bob. J. Geophys. Res. Oceans 118 (5), 2685–2701. https://doi.org/10.1002/jgrc.20207.

van Rijn, L.V., Walstra, D.J.R., Ormondt, M.V., 2004. *Description of TRANSPOR2004 and Implementation in Delft3D-ONLINE.* Deltares (WL).

Wang, P., 2011. Principles of sediment transport applicable in tidal environments. In: Principles of Tidal Sedimentology. Springer Netherlands, Dordrecht, pp. 19–34. https://doi.org/10.1007/978-94-007-0123-6_2.

Wang, H., Chen, Q., Hu, K., Snedden, G.A., Hartig, E.K., Couvillion, B.R., et al., 2017. *Numerical modeling of the effects of Hurricane Sandy and potential future hurricanes on spatial patterns of salt marsh morphology in Jamaica Bay, New York City* (No. 2017-1016). US Geol. Survey. https://doi.org/10.3133/ofr20171016.

Williams, J.J., Esteves, L.S., 2017. Guidance on setup, calibration, and validation of hydrodynamic, wave, and sediment models for shelf seas and estuaries. Adv. Civ. Eng. 2017 (1), 5251902. https://doi.org/10.1155/2017/5251902.

Willmott, C.J., 1981. On the validation of models. Phys. Geogr. 2 (2), 184–194. https://doi.org/10.1080/02723646.1981.10642213.

Xie, D., Hughes, Z., FitzGerald, D., Tas, S., Asik, T.Z., Fagherazzi, S., 2024a. Impacts of climate change on coastal hydrodynamics around a headland and potential headland sediment bypassing. Geophys. Res. Lett. 51. https://doi.org/10.1029/2023GL105323 e2023GL105323.

Xie, D., Hughes, Z., FitzGerald, D., Tas, S., Asik, T.Z., Fagherazzi, S., 2024b. Longshore sediment transport across a tombolo determined by two adjacent circulation cells. J. Geophys. Res. Earth Surf. 129 (10). https://doi.org/10.1029/2024JF007709 e2024JF007709.

Zhang, Z., Chen, C., Song, Z., Zhang, D., Hu, D., Guo, F., 2020. A FVCOM study of the potential coastal flooding in apponagansett bay and clarks cove, Dartmouth Town (MA). Nat. Hazards 103 (3), 2787–2809. https://doi.org/10.1007/s11069-020-04102-9.

Zhu, Q., Wiberg, P.L., 2022. The importance of storm surge for sediment delivery to microtidal marshes. J. Geophys. Res. Earth Surf. 127 (9). https://doi.org/10.1029/2022JF006612 e2022JF006612.